Macroscopic, Freestanding, and Tubular Graphene Architectures Fabricated *via* Thermal Annealing

Duc Dung Nguyen,*,† Seiya Suzuki,† Shuji Kato,‡ Bao Dong To,§ Chia Chen Hsu,§ Hidekazu Murata,‡ Eiji Rokuta,‡ Nyan-Hwa Tai,∥ and Masamichi Yoshimura†

†Toyota Technological Institute, 2-12-1 Hisakata, Tempaku, Nagoya 468-8511, Japan, ‡Faculty of Science and Engineering, Meijo University, 1-501 Shiogamaguchi, Tempaku, Nagoya 468-8502, Japan, §Department of Physics, National Chung Cheng University, Min Hsiung, Chiayi 621, Taiwan, and ∥Department of Materials Science and Engineering, National Tsing-Hua University, Hsinchu 30013, Taiwan

ABSTRACT Manipulation of individual graphene sheets/films into specific architectures at macroscopic scales is crucially important for practical uses of graphene. We present herein a versatile and robust method based on annealing of solid carbon precursors on nickel templates and thermo-assisted removal of poly(methyl methacrylate) under low vacuum of ~0.6 Pa for fabrication of macroscopic, freestanding, and tubular graphene (TG) architectures. Specifically, the TG architectures can be obtained as individual and woven tubes with a diameter of ~50 μm, a wall thickness in the range of 2.1–2.9 nm, a density of ~1.53 mg·cm^{-3}, a thermal stability up to 600 °C in air, an electrical conductivity of ~1.48 × 10^6 S·m^{-1}, and field emission current densities on the order of 10^4 A·cm^{-2} at low applied electrical fields of 0.6–0.7 V·μm^{-1}. These properties show great promise for applications in flexible and lightweight electronics, electron guns, or X-ray tube sources.

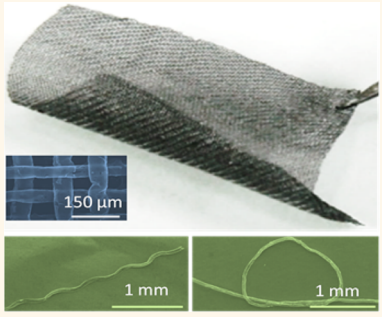

KEYWORDS: macroscopic graphene · graphene tubes · field electron emission · thermal annealing · liquid–liquid separation

Graphene and its derivatives, consisting of fewer than 10 stacked layers of carbon atoms arranged in a honeycomb lattice,[1] possess intriguing thermal, mechanical, and electrical properties.[2–7] Integration of these fascinating properties from individual graphene sheets/films into novel macroscopic architectures is highly imperative for practical uses and opening/exploring their new functions.[8–14] Owing to the advantages of well-developed synthesis, facile processing, and mass production at low cost, chemically converted graphene (CG) nanosheets have been assembled into ingenious configurations such as ultratough papers,[15] transparent conductive films,[16,17] fibers,[18–20] and microtubules[21,22] to expand their uses and achieve advanced applications. Among these, the microtubules prepared by geometric confinement of CG nanosheets under hydrothermal treatment exhibit great benefits of light weight, high strength, good flexibility, and adjustable cavities, which open new potential applications in microfluidics, catalysis, purification, separation, and sensing.[21,22] Nevertheless, the low conductivity nature of CG nanosheets and the large contact resistance induced by intersheet junctions within the assemblies limit their further uses where high electrical performance is required.[8,23] Alternative efforts to obtain a microtubule network, aerographite,[24] by chemical vapor deposition (CVD) using inorganic oxide templates have yielded promising ultralightweight and robust structures. However, these structures are found to be composed of richly disordered sp^2 carbons, that is, low electrical conductivity. In addition, long growth time and massive precipitation of metallic byproduct inside the CVD system may restrict its practical use at an industrial scale. Accordingly, large-area, high-quality, and superior performance graphene films, generally synthesized by thermal annealing or CVD on metal catalytic substrates,[25–28] are obviously desired. However, scalable, sustainable, and controllable construction of these high-performance graphene films into freestanding and tubular architectures at macroscopic scales remains a great challenge.

* Address correspondence to ddnguyen161@gmail.com.

Received for review January 14, 2015 and accepted March 4, 2015.

Published online March 04, 2015
10.1021/acsnano.5b00292

In this study, we present for the first time a versatile and robust method based on rapid annealing of solid carbon precursors on nickel (Ni) templates and thermo-assisted removal of poly(methyl methacrylate) (PMMA) for fabrication of freestanding, tubular graphene (TG) architectures at macroscopic scales. Contrary to structures assembled from tiny and stacked CG nanosheets, our macroscopic TG is a monolith of continuous, large-domain, and high-quality graphene; therefore, superior physical properties are expected. Specifically, the TG architectures can be obtained as individual and woven tubes with a diameter of $\sim$50 μm, a wall thickness in the range of 2.1−2.9 nm, a density of $\sim$1.53 mg·cm^{-3}, a thermal stability up to 600 °C in air, an electrical conductivity of $\sim 1.48 \times 10^6$ S·m^{-1}, and field emission current densities on the order of 10^4 A·cm^{-2} at low applied electrical fields (E) of 0.6−0.7 V·μm^{-1}. These properties show great promise for applications in flexible and lightweight electronics, electron guns, or X-ray tube sources.

RESULTS AND DISCUSSION

Our versatile and robust method relies on the surface precipitation of carbon on Ni[29−33] in combination with thermo-assisted PMMA removal under low-vacuum conditions. The method has advantages of rapid processing, low power consumption, and avoidance of explosive gaseous materials and toxic chemicals. Figure 1 illustrates a procedure for the fabrication processes. In short, a mechanically pressed Ni/cellulose acetate (CA) sample is rapidly heated to a desired temperature under low vacuum. At elevated temperatures, CA-derived carbon atoms/species diffuse into the Ni and subsequently precipitate as graphene on the Ni surfaces during annealing/cooling processes. Through analysis of Raman characteristics of samples annealed at various temperatures, films produced at 950 °C possess few-layer graphene features with the highest degree of graphitic crystallinity (Supporting Information Figure S1) and is thus selected for the TG fabrication processes thereafter. The films on the Ni comprise continuous graphene domains with sizes up to few tens of micrometers; wrinkles and ripples induced by the difference between thermal coefficients of Ni and graphene can be verified by scanning electron microscopy (SEM) observation (Figure S2). In order to obtain the TG, a thin PMMA film is coated on the graphene/Ni wire and serves to maintain the tubular graphene sheath during wet etching of the Ni core wire. Finally, the PMMA film is thermally removed, leading to the formation of TG, a freestanding, extremely large diameter, and ultra-thin-walled graphene tube. It is worth mentioning that the thermo-assisted PMMA removal presented herein is critically important. Employment of conventional acetone-based removal of PMMA[8,27,29] absolutely results in collapsed, unstable, and fragile structures (Figure S3), which are possibly attributed to the liquid capillary force caused by acetone evaporation.[34] On the contrary, using thermal removal helps to avoid the liquid capillary effect, consequently establishing the TG architectures. In addition, this route of PMMA removal could be extensively applied for conventional CVD-derived graphene/Ni wires instead of the annealing-derived graphene/Ni wires in the present study.

The TG can be morphologically designed in various configurations including cantilever-like (Figure 2a), wavy (Figure 2b), and tie-able (Figure 2c) tubes without severe alteration of the tubular structure, suggesting the high mechanical stability. Therefore, specific structures

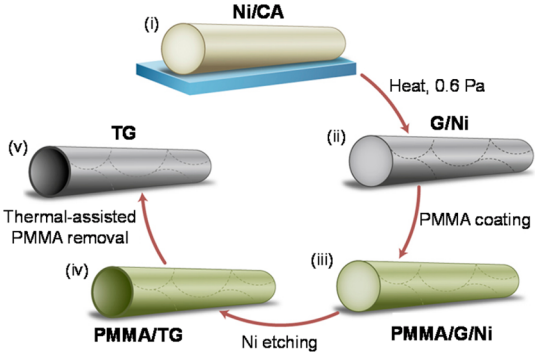

Figure 1. Illustration of the fabrication of a TG structure: (i) Ni wire mechanically pressed with CA membrane (Ni/CA); (ii) graphene sheath formed on Ni core wire (G/Ni) *via* annealing; (iii) PMMA coated on graphene sheath/Ni core wire (PMMA/G/Ni); (iv) PMMA-coated TG (PMMA/TG) produced when etching Ni; (v) freestanding TG achieved after thermal removal of PMMA.

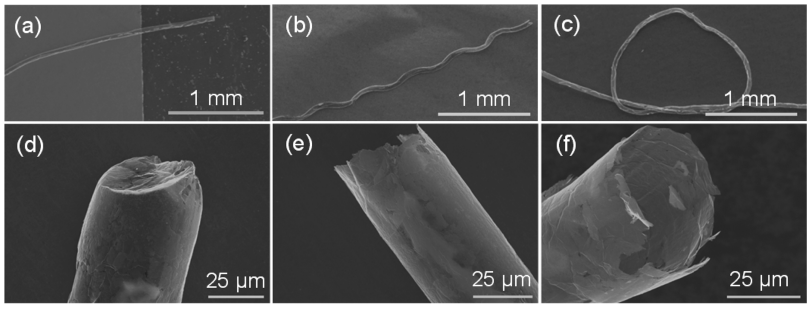

Figure 2. SEM images of individual TGs in various configurations: (a) cantilever-like, (b) wavy, (c) tie-able, (d) closed, and (e,f) open-ended tubes.

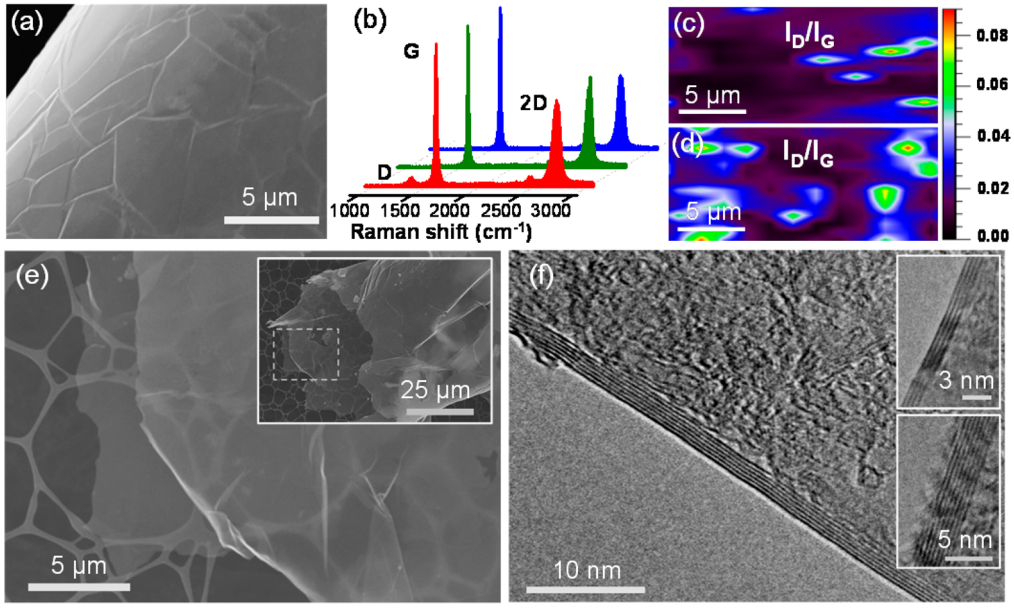

Figure 3. (a) SEM image of the lateral surface of the TG. (b) Typical Raman spectra acquired on the TG surface at different positions. Raman maps of I_D/I_G ratio of the (c) graphene/Ni and (d) TG. (e) SEM image of the tubular edges of a TG on a TEM grid; inset represents an SEM image of the open-ended TG, with the dashed-box area corresponding to part (e) at low magnification. HRTEM images (f and its insets) on the wall edges of the TG.

on demand can be easily conquered *via* manipulation of Ni templates into predetermined shapes followed by the aforementioned fabrication processes. Microscopic SEM examination and energy-dispersive X-ray (EDX) and Raman analyses indicate that inside the TG architectures there exists a carbon whisker, which is probably induced by carbon atoms/species trapped by either cavities or grain grooves inside the Ni during the annealing (Supporting Information Figures S4 and S5). However, this object can be conceptually referred to as a type of impurity as found in carbon nanotube (CNT) materials. Most noteworthy are the graphene-ended caps (Figure 2d), which can be effortlessly opened *via* mechanically cutting the ends of the graphene/Ni wire prior to the Ni etching. Thereby, hollow TG with extremely sharp wall edges are generated (Figure 2e,f), implying numerous potential applications such as electron emitters, microscopic cavities for storing and filling with expedient materials toward multifunctional composites, and high surface area catalyst/supports.[35−41] Furthermore, the TG diameter is finely controlled by Ni wires (Figure S6), while longitudinal regulation of the TG is reliant on the template length. It is envisioned that by utilizing Ni wires with controllable diameters/lengths, a new type of graphene tube with well-defined and predetermined dimensions can be fabricated, consequently providing key materials for advanced technology of graphitic tubes ranging from nanoscopic to macroscopic scales.

The SEM image in Figure 3a shows that lateral surface of the TG consists of continuous micron-sized graphene domains, resembling those of its prototype, the graphene/Ni wire. Raman spectra (Figure 3b) acquired on these domains exhibit features for few-layer graphene, identified as three characteristic peaks, including a D peak at ~1348 cm^{-1}, which is associated with sp^3-hybridized carbon as found in defects or impurities in carbon materials; a G peak at ~1580 cm^{-1}, which results from the E_{2g} vibrational mode of sp^2 carbon; and the 2D peak at ~2704 cm^{-1}, which is the second-order vibration caused by the scattering of phonons at the zone boundary.[30,42,43] The weak intensity of the D peak suggests that the highly graphitic crystallinity of its prototype is thoroughly preserved. This can be further confirmed by a comparison of a D to G peak intensity ratio I_D/I_G, an indication of the degree of graphitic crystallinity. There is no significant increase in the mapped I_D/I_G ratio as the graphene/Ni wire (Figure 3c) evolved to the TG (Figure 3d), implying negligible defects introduced during the fabrication process.

The ultra-thin-wall nature of the TG is obviously proved by the high electron transparency, as revealed by SEM imaging on a tubular edge of an open-ended tube on a copper grid (Figure 3e and its inset). High-resolution transmission electron microscopy (HRTEM) imaging on the wall-edge areas allows observation of layered structure and determination of the number of graphene layers. As shown in Figure 3f and its insets, the TG wall consists of few (4−8) layers of graphene, which is consistent with the Raman features. Additionally, atomic force microscopy (AFM) measurements on an unzipped TG statistically indicate that the wall thickness is mainly distributed in the range of 2.1−2.9 nm, that is, fewer than 10 layers (Supporting Information Figure S7). The variation in thickness

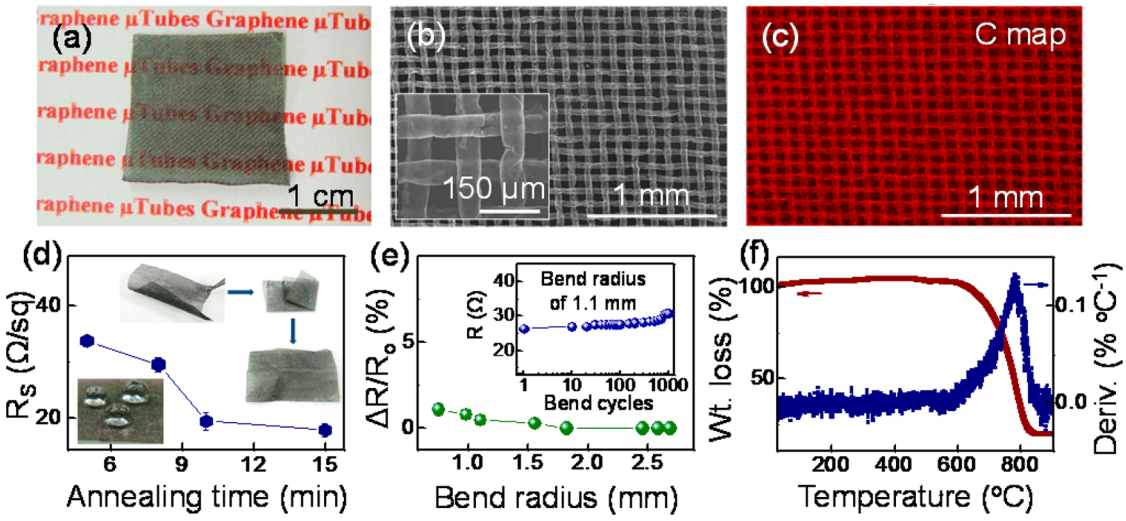

Figure 4. (a) Photograph of a freestanding woven sheet of TGs. (b) SEM image of the woven sheet; inset is a higher-magnification image. (c) EDX map of C element, acquired on the area shown in part (b). (d) Dependence of sheet resistance of the woven TGs on annealing time. In part (d), the lower-left inset is a photograph of water droplets on the woven sheet, and the top-right insets demonstrate the flexibility of the woven TGs. (e) Deviation of electrical resistance of the TG woven sheet under various bend radii; inset shows the deviation under bending cycles. (f) TGA and its first derivative acquired from the woven TGs.

distribution of the TG wall is plausibly attributed to the polycrystalline characteristics of the Ni templates, with which graphene growth on individual Ni grains is self-governing while more layers tend to form nearby grain boundaries.[29] Taking the averaged wall thickness of ~2.4 nm, we determined an electrical conductivity of the TG to be ~1.48 × 10^6 S·m^{-1}, which is comparable to that of CVD few-layer graphene films[44] and is several orders of magnitude higher than those of CG and CNT fibers.[19,45−47]

Notably, the fabrication approach can be extensively employed for construction of macroscopic sheets of woven TGs. The woven sheets are extremely lightweight, mechanically stable, highly conductive, strongly hydrophobic, and vigorously thermo-oxidatively resistant. Similar to the fabrication of individual TGs, the freestanding sheets of woven TGs can be achieved only through the thermo-assisted PMMA removal process; otherwise, collapsed woven structures could be formed (Figure S8). Nevertheless, these collapsed woven structures could be beneficial for use as flexible electrodes when incorporated with or supported by an additional matter.[48]

Figure 4a shows a photograph of a semitransparent, freestanding woven sheet of TGs with a density of ~1.53 mg·cm^{-3}, among those of the lightest materials.[8,11,24] SEM images shown in Figure 4b and its inset indicate that the sheet comprises woven, hollow TGs arranged in a mesh-like structure, mimicking that of the Ni template. Elemental analysis by EDX reveals that the TG woven sheet is mainly composed of carbon (94.0 wt %), as shown in Figure 4c and Supporting Information Figure S9a. Minor quantities of oxygen (4.9 wt %) and iron (1.1 wt %) are probably induced during the low-vacuum annealing and wet Ni etching, respectively (Figure S9b,c). Raman study further confirms that there is no difference in graphitic crystallinity between the individual and woven TGs, thus the woven sheets are anticipated to hold intriguing properties.

As shown in Figure 4d, the woven sheets possess low electrical sheet resistance in the range of 17−40 Ω·sq^{-1}, slightly dependent on the annealing time with which the longer time results in more graphene layers added, consequently decreasing the electrical resistance.[27] Interestingly, the woven sheet exhibits strongly hydrophobic behavior, as signified by water droplets attained in virtually spherical shapes on its surface (lower left inset of Figure 4d). This is attributed to the water-repellent nature of carbon materials and solely microscopic roughness induced by the mesh structure.[9] More importantly, the conducting woven sheets are greatly flexible, bendable, and foldable, as demonstrated in the upper right insets of Figure 4d. In order to evaluate their mechano-electrical durability, a TG woven sheet glued on a polyethylene terephthalate substrate is inspected under bend radii of 0.75−2.68 mm (Figure 4e) and cycle test at a bend radius of 1.10 mm for 1000 times (inset of Figure 4e). When the electrical resistances of the sheet under such bending regimes were probed, there was a slight deviation of ~1% at the bend radius of 0.75 mm and an increase from 26.4 to 30.8 Ω after 1000 cycles, suggesting a great mechanical flexibility of the conducting TG woven sheets.

Thermogravimetric analyses (TGA) reveal that the TG woven sheets are exceedingly resistant to thermal oxidation. Figure 4f shows the TGA curves obtained by heating the woven sheets to 900 °C in dehydrated air and simultaneously recording their weight loss.

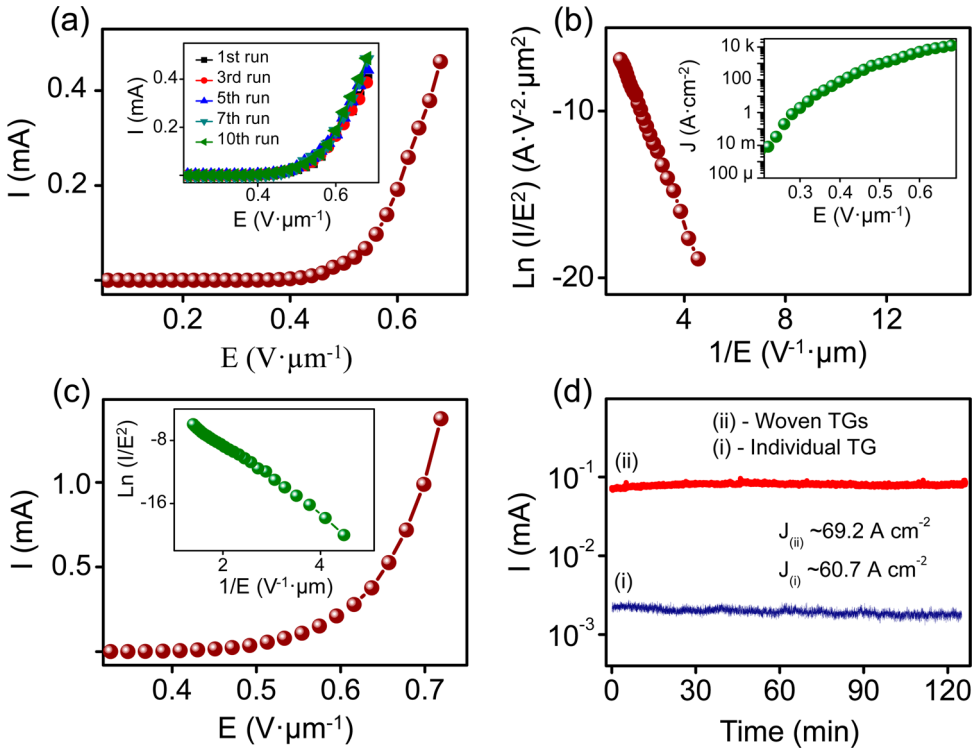

Figure 5. Field electron emission characteristics of the TGs. (a) *I*–*E* curve of the individual TG emitter; inset indicates selected *I*–*E* curves at different cycles. (b) F–N plot of the individual TG emitter; inset is the dependence of current density on applied field. (c) *I*–*E* curve of the woven TG emitter and its corresponding F–N plot (inset). (d) Current stability of the individual and woven TG emitters.

The sheets are stable up to a temperature of ~600 °C and predominantly oxidized at ~785 °C, proving the highly graphitic material. These values of thermo-oxidative resistance are comparable to those of graphite and outperform those of multiwalled CNTs and diamond.[49,50] Raman study also shows that the graphitic crystallinity of the TG woven sheets remains unchanged regardless of being heated at 580 °C in air for hours. The outstanding thermo-oxidative resistance achieved here is ascribed to the high-quality graphene integrated into the very large diameter tubes, that is, low degree of strain, subsequently less reactivity toward oxygen.[49] The woven sheets are thus anticipated to be useful for development of thin composite films, including thermally stable and mechanically flexible conductors, hydrophobic and conductive coatings, and electromagnetic interference shielding sheets for portable electronic devices.

One of the remarkable advantages of the TG architectures is their ultrathin edges on the macroscopically and monolithically graphitic walls, which possess ultrahigh aspect ratio (the ratio of wall lateral size to wall thickness) and a considerably greater number of field electron emitting sites as compared to their analogues on nanoscopic walls (*e.g.*, on CNT walls). Another benefit of the macroscopic TGs is ease of development of highly efficient field emitters. Generally, preparation of an individual nanoscopic emitter is labor-intensive and requires uses of microscopic manipulators/apparatuses for mounting such a tiny tip on a macroscopic electrode *via* a trace of conductive organic glue,[51] that is, high contact resistance. In contrast, due to the macroscopic and freestanding shapes, the preparation of TG emitters with good electrical contact to external electrodes can be effortlessly manipulated and handled without any microscopic tools (Supporting Information Figures S10a,b and S11). With the abundance of emitting sites, large aspect ratio, high electrical conductivity, good mechanical stability, and facile preparation, the macroscopic TG architectures are therefore expected to be promising candidates for field emission sources.

As a proof of concept, the current-applied field characteristics of the TG architectures were investigated under vacuum to evaluate how they would respond as efficient field emitters. Figure 5a presents a typical electron emission current as a function of applied field (I–E curve), recorded from the individual TG emitter. At a low applied field of 0.68 V·μm^{-1}, a very high emission current of ~0.46 mA can be reached, revealing superior performance as compared to that of other remarkable individual emitters, including CNTs (0.1 mA, ~40.0 V·μm^{-1})[52] and tungsten oxide/tungsten hybrid wires (0.17 mA, ~1.5 V·μm^{-1}).[53] To the best of our knowledge, this is the highest reported value for an individual emitting tip at such a low field. The outstanding performance of the individual TG emitter is possibly attributed to the extreme sharpness

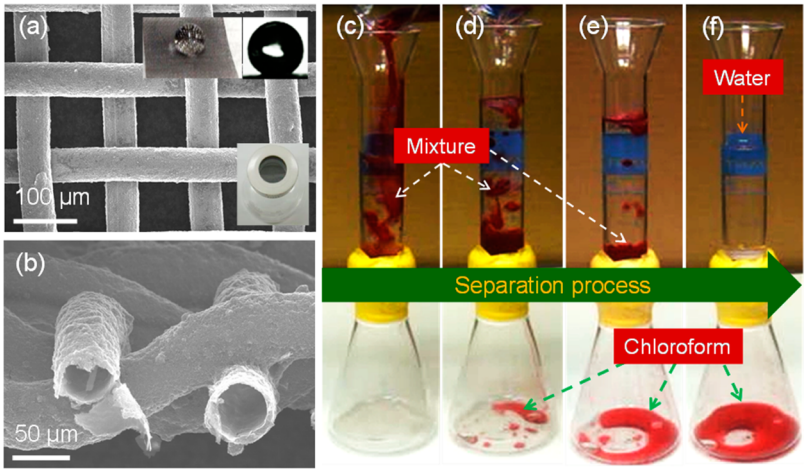

Figure 6. Typical SEM images of (a) a superhydrophobic CNT−graphene/Ni mesh and (b) a tubular CNT−graphene mesh achieved after Ni etching. In part (a), the top-left inset is a photograph of a water droplet attained in a spherical shape on the mesh; the top-right inset is an optical image of a water droplet at a contact angle of 154°, demonstrating the superhydrophobic property. Bottom inset is a photograph indicating the mesh as a separation membrane of a homemade apparatus. (c−f) Snapshots of the water−chloroform (red dyed) separation process.

of the macroscopic wall edge of the monolithic, robust, and highly crystalline graphene tube. This provides an enormous number of effectively emitting sites. Specifically, emitting sites on the tubular wall edge of the TG emitter (wall thickness of ~2.1−2.9 nm, diameter of 50 μm) approximately equal the sum of those from 1000 open-ended, few-walled (~8-walled) CNTs with a diameter of 50 nm. Moreover, these emitting sites are covalently bonded within the monolithic wall, thus much greater emission current can be achieved for the individual TG emitter when compared to either the CNT or a bundle of 1000 CNTs, where intertube junction resistance probably degrades their emission performance. Additionally, good electrical contact could greatly facilitate electron transport from the external electrode (Ni wire) to the graphene wall edge. The inset in Figure 5a shows selected *I*−*E* curves obtained at different cycles, proving the highly repeatable field emission characteristics. As shown in Figure 5b, the linear nature of the Fowler−Nordheim (F−N) plot of $\ln(I/E^2)$ *versus* $1/E$ from the individual TG emitter confirms that the emission process is the tunneling of electrons.[54] Considering that the average wall thickness of the TG emitter is ~2.4 nm, the dependence of current density on the applied field is included in the inset of Figure 5b, where high values on the order of 10^4 A·cm^{-2} were obtained at low *E* of 0.60−0.70 V·μm^{-1}.

In order to achieve greater emission currents, a combination of individual TGs into an integrated emitter, such as a woven TG emitter, is judiciously reasonable. As expected, the *I*−*E* curve obtained from the woven TG emitter (Figure 5c) indicates that a superior emission current of ~1.38 mA can be achieved. The corresponding F−N plot in the inset of Figure 5c and selected *I*−*E* curves (Figure S10c) confirm the genuine field emitter based on the woven TGs with decent repeatability of emission currents. Further *I*−*E* measurements revealed that no emission current could be detected from lateral surfaces of the woven TGs even though *E* increased up to ~8.0 V·μm^{-1} (data not shown), confirming that the high emission current only originated from tubular wall edges.

The threshold field, defined as an applied field at which current density reaches 10 mA·cm^{-2}, of the TG emitters is 0.21−0.27 V·μm^{-1}. By assuming that the work function of the TGs was the same as that of graphite, that is 5.0 eV, we determined the field enhancement factor (β) of the TG-based emitters to be (1.7−1.9) × 10^4. It is worth revealing that field emission performances of the TG emitters are highly competitive with those of the best reported emitters including CNTs, graphene, CNT/graphene hybrids, diamond nanorods, and tungsten oxide nanowires (Table S1).[55−64] Additionally, the TG emitters exhibit good current stability as signified by slight fluctuations surrounding their initial emitting currents of ~0.23 × 10^{-2} mA (individual TG) and ~0.79 × 10^{-1} mA (woven TGs), which correspond to current densities in the range of ~60−70 A·cm^{-2}, as shown in Figure 5d. The current stability is also maintainable when the testing time is extended for days (Figure S10d).

In addition, flexible, conductive, and superhydrophobic meshes composed of CNTs and graphene could be fabricated using our annealing method (Figures S12−S15 and section 3 in the Supporting Information). A potential application of these meshes is separation of the hydrophobic solvents from water. Surface morphology of the CNT−graphene meshes before and after etching the Ni template is revealed using SEM examination (Figure 6a,b and Supporting Information Figures S13 and S14). A dually roughened

surface derived from woven graphene tubes (micro-roughness) and CNT clumps (nano-roughness) can be clearly seen, implying a superhydrophobic surface.[9] Spherical water droplets shown in the top insets of Figure 6a further prove the superhydrophobic behavior; the bottom inset of Figure 6a indicates the location of the mesh, which serves as a liquid−liquid separation membrane of a homemade apparatus. Figure 6c−f shows the snapshots taken during a liquid−liquid separation process. Briefly, a mixture of water/chloroform, where chloroform is dyed red for clearer observation, is poured into the glass funnel of the separation apparatus. Since chloroform has greater density than water, it gradually deposits at the funnel bottom, at which the separation membrane is located. Due to the superhydrophobic nature of the membrane, the chloroform is allowed to flow through and is subsequently collected in the flask below, while water stably stands over the membrane in the funnel; that is, the two liquids are completely separated. This separation membrane is therefore promising for addressing industrial organic pollutants in water for environmental protection.

CONCLUSION

In summary, we have developed a versatile and robust method for the fabrication of macroscopic, freestanding, and tubular graphene architectures with predetermined configurations. The fabrication procedure is facile, sustainable, and forceful to scale up for mass production based on the standard annealing or CVD techniques. As-fabricated architectures possess good mechanical stability, ultralight weight, high electrical conductivity, strong/superhydrophobicity, outstanding thermo-oxidative resistance, and exceptional field emission performance. These properties show great promise for exploring new functions and advancing potential applications of the tubular graphene in flexible and portable electronics, sensors, electron microscopes, X-ray tube sources, and environmental protection. Moreover, using the thermo-assisted PMMA removal presented herein, we strongly believe that a variety of other novel, macro/microscopic, freestanding, hollow graphene structures such as sponges, spheres, cubes, needles, or combined structures can be created for advanced applications.

EXPERIMENTAL SECTION

Fabrication of Macroscopic, Freestanding, and Tubular Graphene Architectures. Ni wires and mesh (NI-311085/NI-311107 and NI-318200, Nilaco) served as catalytic templates for the formation of individual and woven TG architectures. First, the Ni template was cleaned in an acetone bath with ultrasonication for 10 min to eliminate contaminants residing on its surface. Second, the template was rolling-pressed with a cellulose acetate membrane (C045A047A, Advantec), a solid carbon precursor. The resultant sample was then placed in a quartz container, which was located inside a chamber of an infrared lamp annealing system (Mila 5000, Ulvac). At a base vacuum level of ~0.6 Pa, the sample was heated to desired temperatures with a heating rate of 15.0 °C·s^{-1}. After being held at the annealing temperature for 8 min, the sample was cooled to 500 °C at a rate of ~16 °C·s^{-1} and to room temperature within 10 min. Subsequently, the as-annealed sample was immersed in a solution of PMMA (950 A9, MicroChem) in acetone (PMMA/acetone, v/v = 3/5) for 90 min followed by drying overnight at room temperature in a fume hood. This helped to form a thin PMMA film on the annealed sample, consequently serving to maintain the tubular graphene sheath when its Ni core was dissolved by an etching solution of $FeCl_3$/HCl (1 M/1 M). The PMMA-coated tubular graphene sheath was immersed in deionized water several times to thoroughly wash out residues caused by the etchant. Finally, the PMMA film was thermally removed at a temperature of 450 °C and a pressure of ~0.6 Pa for 30 min; consequently, the freestanding TG could be obtained.

Microscopy Characterization. The microscopic morphologies and structures of the TG samples were investigated by field emission scanning electron microscopy (Hitachi S4700 and SU 3500), atomic force microscopy (Multimode 8, Bruker), Raman spectroscopy (Renishaw with a 532 nm laser excitation), and transmission electron microscopy (JEOL JEM-2100). Elemental mapping analysis of the TG samples was performed using an energy-dispersive a Hitachi SU 3500 spectroscope. Wall thickness of the TG was characterized using the AFM operated in peak force tapping mode on an unzipped tube, which was prepared by etching the top half of the graphene sheath on a Ni wire using oxygen plasma followed by removal of the Ni.

Property Measurement. Thermo-oxidative resistance of the TGs was studied with a thermogravimetric analysis apparatus (Shimadzu, DTG-60H) using hydrated air at flow rate of 100 mL·min^{-1} and a heating rate of 10 °C·min^{-1}. Electrical sheet resistances of the TG samples were measured *via* a four-probe method using a dual-channel sourcemeter (Keithley 2636). To measure the electrical resistance under mechanical bending, a two-probe technique was employed. Field electron emission properties of individual and woven open-ended TGs were characterized in a chamber with a base pressure of ~3.0 × 10^{-6} Pa. The spacing between TG emitters and a planar stainless steel anode was 2.5 mm. Emission current was detected using a digital electrometer (8240 ADCMT) connected to a grounded cathode. Before field emission characteristics were recorded, an electrical aging process (voltage swept to 1.0−1.2 kV and held for several minutes) was applied to remove emission noise and instabilities.

Conflict of Interest: The authors declare no competing financial interest.

Acknowledgment. This study was supported in part by a grant of the Support Program for Forming Strategic Research Infrastructure for Private Universities from Ministry of Education, Culture, Sport, Science and Technology, Japan (MEXT).

Supporting Information Available: Details regarding SEM images, EDX/AFM/Raman data, additional field emission results, and development of superhydrophobic CNT−graphene-based meshes. This material is available free of charge *via* the Internet at http://pubs.acs.org.

REFERENCES AND NOTES

1. Geim, A. K.; Novoselov, K. S. The Rise of Graphene. *Nat. Mater.* **2007**, *6*, 183–191.
2. Balandin, A. A.; Ghosh, S.; Bao, W.; Calizo, I.; Teweldebrhan, D.; Miao, F.; Lau, C. N. Superior Thermal Conductivity of Single-Layer Graphene. *Nano Lett.* **2008**, *8*, 902–907.

3. Shih, C. J.; Vijayaraghavan, A.; Krishnan, R.; Sharma, R.; Han, J. H.; Ham, M. H.; Jin, Z.; Lin, S.; Paulus, G. L. C.; Reuel, N. F.; et al. Bi- and Trilayer Graphene Solutions. *Nat. Nanotechnol.* **2011**, *6*, 439–445.
4. Lee, G. H.; Cooper, R. C.; An, S. J.; Lee, S.; Zande, A.; Petrone, N.; Hammerberg, A. G.; Lee, C.; Crawford, B.; Oliver, W.; et al. High-Strength Chemical-Vapor-Deposited Graphene and Grain Boundaries. *Science* **2013**, *340*, 1073–1076.
5. Lui, C. H.; Ye, Z.; Keiser, C.; Xiao, X.; He, R. Temperature-Activated Layer-Breathing Vibrations in Few-Layer Graphene. *Nano Lett.* **2014**, *14*, 4615–4621.
6. Geim, A. K.; Morozov, S. V.; Jiang, D.; Zhang, Y.; Dubonos, S. V.; Grigorieva, I. V.; Firsov, A. A. Electric Field Effect in Atomically Thin Carbon Films. *Science* **2004**, *306*, 666–669.
7. Novoselov, K. S.; Geim, A. K.; Morozov, S. V.; Jiang, D.; Katsnelson, M. I.; Grigorieva, I. V.; Dubonos, S. V.; Firsov, A. A. Two-Dimensional Gas of Massless Dirac Fermions in Graphene. *Nature* **2005**, *438*, 197–200.
8. Chen, Z.; Ren, W.; Gao, L.; Liu, B.; Pei, S.; Cheng, H. M. Three-Dimensional Flexible and Conductive Interconnected Graphene Networks Grown by Chemical Vapour Deposition. *Nat. Mater.* **2011**, *10*, 424–428.
9. Nguyen, D. D.; Tai, N. H.; Lee, S. B.; Kuo, W. S. Superhydrophobic and Superoleophilic Properties of Graphene-Based Sponges Fabricated Using a Facile Dip Coating Method. *Energy Environ. Sci.* **2012**, *5*, 7908–7912.
10. Yan, H.; Li, X.; Chandra, B.; Tulevski, G.; Wu, Y.; Freitag, M.; Zhu, W.; Avouris, P.; Xia, F. Tunable Infrared Plasmonic Devices Using Graphene/Insulator Stacks. *Nat. Nanotechnol.* **2012**, *7*, 330–334.
11. Hu, H.; Zhao, Z.; Wan, W.; Gogotsi, Y.; Qiu, J. Ultralight and Highly Compressible Graphene Aerogels. *Adv. Mater.* **2013**, *25*, 2219–2223.
12. Yang, X.; Cheng, C.; Wang, Y.; Qiu, L.; Li, D. Liquid-Mediated Dense Integration of Graphene Materials for Compact Capacitive Energy Storage. *Science* **2013**, *341*, 534–537.
13. Chen, Z.; Xu, C.; Ma, C.; Ren, W.; Cheng, H. M. Lightweight and Flexible Graphene Foam Composites for High-Performance Electromagnetic Interference Shielding. *Adv. Mater.* **2013**, *25*, 1296–1300.
14. Joshi, R. K.; Carbone, P.; Wang, F. C.; Kravets, V. G.; Su, Y.; Grigorieva, I. V.; Wu, H. A.; Geim, A. K.; Nair, R. R. Precise and Ultrafast Molecular Sieving through Graphene Oxide Membranes. *Science* **2014**, *343*, 752–754.
15. Dikin, D. A.; Stankovich, S.; Zimney, E. J.; Piner, R. D.; Dommett, G. H. B.; Evmenenko, G.; Nguyen, S. B. T.; Ruoff, R. S. Preparation and Characterization of Graphene Oxide Paper. *Nature* **2007**, *448*, 457–460.
16. Eda, G.; Fanchini, G.; Chhowalla, M. Large-Area Ultrathin Films of Reduced Graphene Oxide as a Transparent and Flexible Electronic Material. *Nat. Nanotechnol.* **2008**, *3*, 270–274.
17. Li, X.; Zhang, G.; Bai, X.; Sun, X.; Wang, X.; Wang, E.; Dai, H. Highly Conducting Graphene Sheets and Langmuir–Blodgett Films. *Nat. Nanotechnol.* **2008**, *3*, 538–542.
18. Yun, Y. J.; Hong, W. G.; Kim, W. J.; Jun, Y.; Kim, B. H. A Novel Method for Applying Reduced Graphene Oxide Directly to Electronic Textiles from Yarns to Fabrics. *Adv. Mater.* **2013**, *25*, 5701–5705.
19. Cao, J.; Zhang, Y.; Men, C.; Sun, Y.; Wang, Z.; Zhang, X.; Li, Q. Programmable Writing of Graphene Oxide/Reduced Graphene Oxide Fibers for Sensible Networks with *In Situ* Welded Junctions. *ACS Nano* **2014**, *8*, 4325–4333.
20. Silva, R. C.; Gomez, A. M.; Kim, H.; Jang, H.; Tristan, F.; Diaz, S. V.; Rajukumar, L. P.; Elias, A. L.; Lopez, N. P.; Suhr, J.; et al. Super-stretchable Graphene Oxide Macroscopic Fibers with Outstanding Knotability Fabricated by Dry Film Scrolling. *ACS Nano* **2014**, *8*, 5959–5967.
21. Hu, C.; Zhao, Y.; Cheng, H.; Wang, Y.; Dong, Z.; Jiang, C.; Zhai, X.; Jiang, L.; Qu, L. Graphene Microtubings: Controlled Fabrication and Site-Specific Functionalization. *Nano Lett.* **2012**, *12*, 5879–5884.
22. Zhao, Y.; Jiang, C.; Hu, C.; Dong, Z.; Xue, J.; Meng, Y.; Zheng, N.; Chen, P.; Qu, L. Large-Scale Spinning Assembly of Neat, Morphology-Defined, Graphene-Based Hollow Fibers. *ACS Nano* **2013**, *7*, 2406–2412.
23. Park, S.; Ruoff, R. S. Chemical Methods for the Production of Graphenes. *Nat. Nanotechnol.* **2009**, *4*, 217–224.
24. Mecklenburg, M.; Schuchardt, A.; Mishra, Y. K.; Kaps, S.; Adelung, R.; Lotnyk, A.; Kienle, L.; Schulte, K. Aerographite: Ultra Lightweight, Flexible Nanowall, Carbon Microtube Material with Outstanding Mechanical Performance. *Adv. Mater.* **2012**, *24*, 3486–3490.
25. Li, X.; Cai, W.; An, J.; Kim, S.; Nah, J.; Yang, D.; Piner, R.; Velamakanni, A.; Jung, I.; Tutuc, E.; et al. Large-Area Synthesis of High-Quality and Uniform Graphene Films on Copper Foils. *Science* **2009**, *324*, 1312–1314.
26. Sun, Z.; Yan, Z.; Yao, J.; Beitler, E.; Zhu, Y.; Tour, J. M. Growth of Graphene from Solid Carbon Sources. *Nature* **2010**, *468*, 549–552.
27. Bae, S.; Kim, H.; Lee, Y.; Xu, X.; Park, J. S.; Zheng, Y.; Balakrishnan, J.; Lei, T.; Kim, H. R.; Song, Y. I.; et al. Roll-to-Roll Production of 30-Inch Graphene Films for Transparent Electrodes. *Nat. Nanotechnol.* **2010**, *5*, 574–578.
28. Peng, Z.; Yan, Z.; Sun, Z.; Tour, J. M. Direct Growth of Bilayer Graphene on SiO_2 Substrates by Carbon Diffusion through Nickel. *ACS Nano* **2011**, *5*, 8241–8247.
29. Reina, A.; Jia, X.; Ho, J.; Nezich, D.; Son, H.; Bulovic, V.; Dresselhaus, M. S.; Kong, J. Large Area, Few-Layer Graphene Films on Arbitrary Substrates by Chemical Vapor Deposition. *Nano Lett.* **2009**, *9*, 30–35.
30. Kim, K. S.; Zhao, Y.; Jang, H.; Lee, S. Y.; Kim, J. M.; Kim, K. S.; Ahn, J. H.; Kim, P.; Choi, J. Y.; Hong, B. H. Large-Scale Pattern Growth of Graphene Films for Stretchable Transparent Electrodes. *Nature* **2009**, *457*, 706–710.
31. Kato, T.; Hatakeyama, R. Site- and Alignment-Controlled Growth of Graphene Nanoribbons from Nickel Nanobars. *Nat. Nanotechnol.* **2012**, *7*, 651–656.
32. Nguyen, D. D.; Tiwari, R. N.; Matsuoka, Y.; Hashimoto, G.; Rokuta, E.; Chen, Y. Z.; Chueh, Y. L.; Yoshimura, M. Low Vacuum Annealing of Cellulose Acetate on Nickel towards Transparent Conductive CNT–Graphene Hybrid Films. *ACS Appl. Mater. Interfaces* **2014**, *6*, 9071–9077.
33. Ago, H.; Tanaka, I.; Ogawa, Y.; Yunus, R. M.; Tsuji, M.; Hibino, H. Lattice-Oriented Catalytic Growth of Graphene Nanoribbons on Heteroepitaxial Nickel Films. *ACS Nano* **2013**, *7*, 10825–10833.
34. Futaba, D. N.; Hata, K.; Yamada, T.; Hiraoka, T.; Hayamizu, Y.; Kakudate, Y.; Tanaike, O.; Hatori, H.; Yumura, M.; Iijima, S. Shape-Engineerable and Highly Densely Packed Single-Walled Carbon Nanotubes and Their Application as Supercapacitor Electrodes. *Nat. Mater.* **2006**, *5*, 987–994.
35. Rinzler, A. G.; Hafner, J. H.; Nikolaev, P.; Nordlander, P.; Colbert, D. T.; Smalley, R. E.; Lou, L.; Kim, S. G.; Tománek, D. Unraveling Nanotubes: Field Emission from an Atomic Wire. *Science* **1995**, *269*, 1550–1553.
36. Zhou, G.; Duan, W.; Gu, B. Electronic Structure and Field-Emission Characteristics of Open-Ended Single-Walled Carbon Nanotubes. *Phys. Rev. Lett.* **2001**, *87*, 095504.
37. Dillon, A. C.; Jones, K. M.; Bekkedahl, T. A.; Kiang, C. H.; Bethune, D. S.; Heben, M. J. Storage of Hydrogen in Single-Walled Carbon Nanotubes. *Nature* **1997**, *386*, 377–379.
38. Sloan, J.; Terrones, M.; Nufer, S.; Friedrichs, S.; Bailey, R. S.; Woo, H. G.; Ruhle, M.; Hutchison, J. L.; Green, M. L. H. Metastable One-Dimensional $AgCl_{1-x}I_x$ Solid-Solution Wurzite "Tunnel" Crystals Formed within Single-Walled Carbon Nanotubes. *J. Am. Chem. Soc.* **2002**, *124*, 2116–2117.
39. Hu, J.; Bando, Y.; Zhan, J.; Zhi, C.; Golberg, D. Carbon Nanotubes as Nanoreactors for Fabrication of Single-Crystalline Mg_3N_2 Nanowires. *Nano Lett.* **2006**, *6*, 1136–1140.
40. Maniwa, Y.; Matsuda, K.; Kyakuno, H.; Ogasawara, S.; Hibi, T.; Kadowaki, H.; Suzuki, S.; Achiba, Y.; Kataura, H. Water-Filled Single-Wall Carbon Nanotubes as Molecular Nanovalves. *Nat. Mater.* **2007**, *6*, 135–141.
41. Liang, Y.; Li, Y.; Wang, H.; Zhou, J.; Wang, J.; Regier, T.; Dai, H. Co_3O_4 Nanocrystals on Graphene as a Synergistic Catalyst for Oxygen Reduction Reaction. *Nat. Mater.* **2011**, *10*, 780–786.

42. Ferrari, A. C.; Meyer, J. C.; Scardaci, V.; Casiraghi, C.; Lazzeri, M.; Mauri, F.; Piscanec, S.; Jiang, D.; Novoselov, K. S.; Roth, S.; et al. Raman Spectrum of Graphene and Graphene Layers. *Phys. Rev. Lett.* **2006**, *97*, 187401.
43. Malard, L. M.; Pimenta, M. A.; Dresselhaus, G.; Dresselhaus, M. S. Raman Spectroscopy in Graphene. *Phys. Rep.* **2009**, *473*, 51–87.
44. Chen, S.; Cai, W.; Piner, R. D.; Suk, J. W.; Wu, Y.; Ren, Y.; Kang, J.; Ruof, R. S. Synthesis and Characterization of Large-Area Graphene and Graphite Films on Commercial Cu–Ni Alloy Foils. *Nano Lett.* **2011**, *11*, 3519–3525.
45. Dong, Z.; Jiang, C.; Cheng, H.; Zhao, Y.; Shi, G.; Jiang, L.; Qu, L. Facile Fabrication of Light, Flexible and Multifunctional Graphene Fibers. *Adv. Mater.* **2012**, *24*, 1856–1861.
46. Vigolo, B.; Pénicaud, A.; Coulon, C.; Sauder, C.; Pailler, R.; Journet, C.; Bernier, P.; Poulin, P. Macroscopic Fibers and Ribbons of Oriented Carbon Nanotubes. *Science* **2000**, *290*, 1331–1334.
47. Davis, V.; Vasquez, A. P.; Green, M.; Rai, P.; Behabtu, N.; Prieto, V.; Booker, R.; Schmidt, V.; Kesselman, E.; Zhou, W.; et al. True Solutions of Single-Walled Carbon Nanotubes for Assembly into Macroscopic Materials. *Nat. Nanotechnol.* **2009**, *4*, 830–834.
48. Zang, X.; Chen, Q.; Li, P.; He, Y.; Li, X.; Zhu, M.; Li, X.; Wang, K.; Zhong, M.; Wu, D.; et al. Highly Flexible and Adaptable, All-Solid-State Supercapacitors Based on Graphene Woven-Fabric Film Electrodes. *Small* **2014**, *10*, 2583–2588.
49. Bom, D.; Andrews, R.; Jacques, D.; Anthony, J.; Chen, B.; Meier, M. S.; Selegue, J. P. Thermogravimetric Analysis of the Oxidation of Multiwalled Carbon Nanotubes: Evidence for the Role of Defect Sites in Carbon Nanotube Chemistry. *Nano Lett.* **2002**, *2*, 615–619.
50. Lin, W.; Moon, K. S.; Zhang, S.; Ding, Y.; Shang, J.; Chen, M.; Wong, C. Microwave Makes Carbon Nanotubes Less Defective. *ACS Nano* **2010**, *4*, 1716–1722.
51. Heeres, E. C.; Bakkers, E. P. A. M.; Roest, A. L.; Kaiser, M.; Oosterkamp, T. H.; Jonge, N. D. Electron Emission from Individual Indium Arsenide Semiconductor Nanowires. *Nano Lett.* **2007**, *7*, 536–540.
52. Minoux, E.; Groening, O.; Teo, K. B. K.; Dalal, S. H.; Gangloff, L.; Schnell, J. P.; Hudanski, L.; Bu, I. Y. Y.; Vincent, P.; Legagneux, P.; et al. Achieving High-Current Carbon Nanotube Emitters. *Nano Lett.* **2005**, *5*, 2135–2138.
53. Seelaboyina, R.; Huang, J.; Park, J.; Kang, D. H.; Choi, W. B. Multistage Field Enhancement of Tungsten Oxide Nanowires and Its Field Emission in Various Vacuum Conditions. *Nanotechnology* **2006**, *17*, 4840–4844.
54. Fowler, R. H.; Nordheim, L. Electron Emission in Intense Electric Fields. *Proc. R. Soc. A* **1928**, *119*, 173–181.
55. Fan, S.; Chapline, M. G.; Franklin, N. R.; Tombler, T. W.; Cassell, A. M.; Dai, H. Self-Oriented Regular Arrays of Carbon Nanotubes and Their Field Emission Properties. *Science* **1999**, *283*, 512–514.
56. López, N. P.; Plata, B. R.; León, J. A. B.; Gómez, A. M.; Cruz, D. H.; Hirata, G. A.; Meunier, V.; Méndez, A. R. B.; Charlier, J. C.; Maruyama, B.; et al. Millimeter-Long Carbon Nanotubes: Outstanding Electron-Emitting Sources. *ACS Nano* **2011**, *5*, 5072–5077.
57. Wu, Z. S.; Pei, S.; Ren, W.; Tang, D.; Gao, L.; Liu, B.; Li, F.; Liu, C.; Chen, H. M. Field Emission of Single-Layer Graphene Films Prepared by Electrophoretic Deposition. *Adv. Mater.* **2009**, *21*, 1756–1760.
58. Jiang, L.; Yang, T.; Liu, F.; Dong, J.; Yao, Z.; Shen, C.; Deng, S.; Xu, N.; Liu, Y.; Gao, H. J. Controlled Synthesis of Large-Scale, Uniform, Vertically Standing Graphene for High-Performance Field Emitters. *Adv. Mater.* **2013**, *25*, 250–255.
59. Ye, D.; Moussa, S.; Ferguson, J. D.; Baski, A. A.; El-Shall, M. S. Highly Efficient Electron Field Emission from Graphene Oxide Sheets Supported by Nickel Nanotip Arrays. *Nano Lett.* **2012**, *12*, 1265–1268.
60. Yan, Z.; Ma, L.; Zhu, Y.; Lahiri, I.; Hahm, M. H.; Liu, Z.; Yang, S.; Xiang, C.; Lu, W.; Peng, Z.; et al. Three-Dimensional Metal-Graphene-Nanotube Multifunctional Hybrid Materials. *ACS Nano* **2013**, *7*, 58–64.
61. Lee, D. H.; Kim, J. E.; Han, T. H.; Hwang, J. W.; Jeon, S.; Choi, S. Y.; Hong, S. H.; Lee, W. J.; Ruoff, R. S.; Kim, S. O. Versatile Carbon Hybrid Films Composed of Vertical Carbon Nanotubes Grown on Mechanically Compliant Graphene Films. *Adv. Mater.* **2010**, *22*, 1247–1252.
62. Deng, J. H.; Zheng, R. T.; Zhao, Y.; Cheng, G. A. Vapor–Solid Growth of Few-Layer Graphene Using Radio Frequency Sputtering Deposition and Its Application on Field Emission. *ACS Nano* **2012**, *6*, 3727–3733.
63. Shang, N.; Papakonstantinou, P.; Wang, P.; Zakharov, A.; Palnitkar, U.; Lin, I. N.; Chu, M.; Stamboulis, A. Self-Assembled Growth, Microstructure, and Field-Emission High-Performance of Ultrathin Diamond Nanorods. *ACS Nano* **2009**, *3*, 1032–1038.
64. Zhang, X.; Gong, L.; Liu, K.; Cao, Y.; Xiao, X.; Sun, W.; Hu, X.; Gao, Y.; Chen, J.; Zhou, J.; et al. Tungsten Oxide Nanowires Grown on Carbon Cloth as a Flexible Cold Cathode. *Adv. Mater.* **2010**, *22*, 5292–5296.